Review

Palladium effect over Mo and NiMo/alumina–titania sulfided catalysts on the hydrodesulfurization of 4,6-dimethyldibenzothiophene

A. Aguirre-Gutiérrez [a], J.A. Montoya de la Fuente [a,*], J.A. de los Reyes [b], P. del Angel [a], A. Vargas [a]

[a] Instituto Mexicano del Petróleo, Dirección de Investigación y Posgrado, Eje Central Lázaro Cárdenas 152, 07730 San Bartolo Atepehuacan, México, DF, Mexico
[b] Universidad Autónoma Metropolitana-Iztapalapa, Área de Ingeniería Química, Av. FFCC R, Atlixco No. 186, Col. Vicentina, Iztapalapa, 09340, México, DF, Mexico

ARTICLE INFO

ABSTRACT

The influence of Pd as additive for Ni and Mo catalysts supported on alumina–titania (Mo/AT) sulfided catalysts was investigated in the hydrodesulfurization of 4,6-dimethyldibenzothiophene. Pd incorporation was carried out in the oxidic phases by using sequential impregnation. The alumina–titania support was formed by anatase–TiO_2 crystallites randomly dispersed on γ-Al_2O_3. Characterization by X-ray diffraction and Raman spectroscopy revealed that MoOx species for PdMo supported on alumina–titania displayed larger particles than those in PdNiMo catalysts. HRTEM images showed an increase in order and stacking for MoS_2 slabs after Pd addition to NiMo samples, as compared with Mo/AT. Pd incorporation over the NiMo/AT sample increased the reaction rate by 30% while no significant increase was recorded for the PdMo sample. This value corresponds to the most active catalyst and it points out to a promoting effect by Pd. This prominent hydrodesulfurization capacity for the PdNiMo/AT suggests a close interaction of Pd with NiMo. Furthermore, since Pd promoted the HDS activity for a NiMo system, the alumina–titania support played an important role.

© 2011 Elsevier B.V. All rights reserved.

Contents

1. Introduction

The conventional hydrodesulfurization catalysts CoMo or NiMo supported on γ-alumina have been widely used in the hydrodesulfurization (HDS) processes. The removal of sulfur from fuels has been of paramount importance to diminish air polluting emissions of sulfur dioxide which contribute to acid rain. Due to increasingly stringent environmental legislations on the sulfur content (<15 ppm) for diesel derived from middle distillates, the traditional catalysts and HDS process technologies will not satisfy the requirements in the so-called ultra-deep HDS [1]. An additional problem arises from the fact that a significant part of the oil reserves in the world is comprised of heavy crudes containing high concentration of sulfur, nitrogen, aromatics and metals such as Ni, Fe and V. These raw feeds for diesel production have become heavier with higher sulfur and nitrogen concentrations.

* Corresponding author. Tel.: +52 55 91758375.
  E-mail address: amontoya@imp.mx (J.A.M. de la Fuente).

It has been established that the most refractory compounds found in diesel cuts are alkyl-substituted dibenzothiophenes (DBT) with alkyl groups in the positions close to the sulfur atom (positions 4 and 6) and the HDS reaction may follow two main pathways: hydrogenolysis (DDS) and hydrogenation (HYD), where the latter is generally the dominating pathway over commercial Mo-based catalysts [1,2]. As published earlier, supported precious metals might be suitable catalysts for deep HDS, starting with a feed containing 200 ppm or less, because these metals exhibit higher hydrogenation activities than metal sulfides [1]. However, noble metal crystallites are highly sensitive to the presence of sulfur-containing molecules and they could transform into less active metal sulfide particles.

Several papers in the literature have dealt with Pt supported on acidic materials in order to improve the resistance to sulfur poisoning [3]. It has been reported that acidity of the support produces electron deficient metallic particles and these are highly resistant to sulfur poisoning. Nevertheless, acidic supports could lead to excessive cracking products and low cetane numbers for diesel [3,4]. Thus, several strategies can be envisaged to decrease this property such as the addition of rare earth elements to zeolitic carriers [4] or the substitution of SiO_2-based supports by reducible or semiconductor oxides [5,6]. In this line, alumina–titania mixed oxides have been studied as alternative carriers for Pt or Pd-based catalysts. It has been evidenced that Pt, Pd and Pt–Pd catalysts modified their activity owing to a different interaction with alumina–titania mixed oxides [5] when compared to alumina-supported samples. A Pd–Pt catalyst supported on alumina–titania with an equimolar composition displayed the highest HDS activity. Besides, Nuñez et al. [6] focused their work on the evaluation in the HYD of biphenyl (BP) in the presence of sulfur for Al_2O_3–TiO_2 supported PdPt catalysts, varying the Ti content in the carrier. They concluded that the presence of Ti in the samples increased the HYD activity as a result of changes in the electronic properties of the active phase. Moreover, Ti increased the sulfur resistance of the metallic particles under HYD conditions. Thus, Al_2O_3–TiO_2 possesses an interesting potential as support for Pd or Pt-based catalysts.

Another approach to overcome the low reactivity of 4,6-DMDBT has been undertaken for instance by favoring the hydrogenation pathway. As a result, several groups have investigated the incorporation of small amounts of single noble metals, Ru, Pt, Pd or bimetallic Pt–Pd to conventional Mo, CoMo or NiW sulfided catalysts [7–15]. Modification of conventional Mo or CoMo/Al_2O_3 systems by noble metals led to a significant improvement in HDS and HYD of DBT, HDN of pyridine and HYD of cyclohexene and naphthalene and synergetic effects for bimetallic PtMo and PtRu catalysts were found depending on the synthesis procedure [7–9]. For instance, a high activity was found when noble metal was incorporated into the sulfided Mo phase [7].

More recently, Pessayre et al. [13] examined the effect of the addition of Pt on three industrial sulfided catalysts, CoMo, NiMo and NiW supported on alumina. In all cases, a 20–40% increase in the catalytic hydrogenation activity was observed when Pt was added after the sulfidation of the commercial catalysts. In that case, the catalytic properties seem to correspond to the addition of the properties of each component. On the contrary, when Pt was impregnated on the oxidic form of the catalyst a sharp decrease in the activity was observed. The above can be explained in terms of the several kinds of interactions between Pt and Mo or W components depending on Mo or W concentrations, such kind of interaction may prevent the formation of some highly active so-called "CoMoS" or "NiWS" entities. Therefore, the benefit of the sulfidation for the formation of "CoMoS" is kept even after impregnation of the Pt, indicating that the negative effect originated from the interaction with the oxidic species. The authors conclude that, in order to keep the additive effect, only a small content of Pt must be added. By contrast, Navarro et al. [14] modified commer-

Table 1
Catalysts nominal metals loading.

Catalyst	Mo (atoms/nm)	Ni (atoms/nm)	Ni Ni/(Ni + Mo)	Pd (atoms/nm)
Mo/A	3.6	–	–	–
NiMo/A	3.6	1.54	0.3	–
PdNiMo/A	3.6	1.54	0.3	0.087
Mo/AT	3.6	–	–	–
Pd/AT	–	–	–	0.087
PdMo/AT	3.6	–	–	0.087
NiMo/AT	3.6	1.54	0.3	–
PdNiMo/AT	3.6	1.54	0.3	0.087

cial Ni(Co)Mo/γ-alumina catalysts by the addition of Pd and Ru in order to enhance their hydrogenation function. They reported that the sulfide ternary catalysts based on the NiMo system were found to be more active in the HDS of DBT than those based on CoMo formulation. Besides, Klimova et al. [15] inquired into the possibility of increasing the HYD ability of conventional NiMo/γ-Al_2O_3 catalyst by the incorporation of different noble metals (NM = Pt, Pd, Ru), founding that Pt and Pd-containing ternary catalysts showed activity 10–20% higher than a conventional NiMo/γ-Al_2O_3 sample. In this work, metal particles exhibited higher particle sizes as compared with published results, suggesting low dispersion of the precious metals.

Therefore, in spite of the relative disagreement in published work, noble metals addition to conventional NiMo or NiW catalysts seems to be an interesting way to improve deep HDS catalytic activities. Furthermore, the modification of the carrier by a semi-conductor oxide would contribute positively to this task. In the present work, the influence of adding Pd and Ni to Mo oxide supported on alumina–titania over the hydrodesulfurization of 4,6-DMDBT was investigated and the characterization of the structure and surface of the calcined and sulfided catalysts was carried out, in order to correlate their physicochemical proprieties to the catalytic behavior.

2. Experimental

2.1. Catalysts preparation

Series of Mo, Pd, NiMo and PdNiMo catalysts supported on γ-Al_2O_3 and titania-modified alumina were prepared in order to evaluate the effect of the TiO_2 incorporation over Al_2O_3. The γ-Al_2O_3 was an industrial carrier (surface area = 240 m^2/g, pore volume = 0.7 cm^3/g, pore diameter = 8.5 nm), referred as A and the alumina–titania support (surface area = 195 m^2/g, pore volume = 0.7 cm^3/g, pore diameter = 8.6 nm) contained 6 wt.% TiO_2 in its formulation, hereafter referred as AT. The transition metal ionic species deposition was made by successive incipient wetness impregnation method. The nominal compositions of the series of catalysts are shown in Table 1. The atomic ratio of Ni promoter was fixed as Ni/(Ni + Mo) = 0.3, which was found to be the optimum value for industrial NiMo/Al_2O_3 solids [1,2]. Pd loading was 0.3 wt%, equivalent to the atomic ratio Pd/(Pd + Mo) = 0.087. Catalysts were prepared using ammonium heptamolybdate, $(NH_4)_6Mo_7O_{24}·4H_2O$ from Sigma ACS; palladium nitrate, $Pd(NO_3)_2·H_2O$ from Aldrich Chem Co.; nickel nitrate, $Ni(NO_3)_2·6H_2O$ from Sigma–Aldrich as precursors.

Prior to impregnation, carriers were sieved (80–100 mesh) and dried at 200 °C during 24 h. Molybdenum was first impregnated at the corresponding concentration, as a second step, Ni or Pd was impregnated. For the PdNiMo/AT catalyst Ni was the second incorporated metal and Pd was impregnated lastly. After each metal impregnation step, the catalysts were dried in an oven at 60 °C dur-

ing 24 h. Finally, the catalysts were calcined at 400 °C for 6 h, with a heating rate of 1 °C/min in a static atmosphere.

Catalysts sulfidation was carried out in a microflow fixed bed U type reactor at 400 °C during 1 h at atmospheric pressure under 4 L/h by using a 15% H_2S/H_2 mixture (PRAXAIR). After the catalyst activation procedure, samples were cooled down under an H_2S/H_2 atmosphere and then flushed with N_2. Samples were kept under an Ar environment until its catalytic evaluation.

2.2. Characterization techniques

Before the preparation of the catalysts, the alumina–titania support was characterized by X-ray diffraction (XRD). These measurements were performed with a D8 Discover with Gadds Bruker system and a Cu K$\alpha_{1,2}$ radiation was used. The correction of the broadening reflections was carried out by using the corundum 1976 NIST. It is important to notice that the anatase–TiO$_2$ (1 0 1) reflection appears especially intense due to the small X-ray beam (500 μm) used in the experiment, which is able to detect crystallites in a low concentration on the (-Al$_2$O$_3$ matrix, as if TiO$_2$ were a contaminant. After the catalyst sufidation process an aliquot of the catalysts were loaded into the X-ray sample holder and covered with a mylar film which is transparent to the X-ray in order to avoid the oxidation of the sulfided samples.

Raman spectroscopy is a very sensitive technique for determining the presence of titanium dioxides, due to the strength of the Raman modes of these compounds. Raman spectra were obtained using an Yvon Jobin Horiba (T64000) spectrometer equipped with a confocal microscope (Olympus, BX41) with an argon ion laser operating at 514.5 nm at a power level of 10 mW. The spectrometer is equipped with a CCD camera detector.

High resolution transmission electron microscopy (HRTEM) technique was used to characterize the aggregation state, shape and size of the nanoparticles of the alumina–titania support (AT) and the sulfided catalysts (Mo/AT, PdMo/AT, NiMo/AT, and PdNiMo/AT). Transmission electron microscopy measurements were performed on a JEOL JEM2200FS (200 kV, point to point resolution 0.195 nm) attached with an EDS Noran detector for chemical analysis.

X-ray photoelectron spectroscopy (XPS) technique was used in order to study the surface chemical composition, dispersion and the oxidation state of the Mo, Ti, Ni and Pd for calcined and sulfided catalysts. XPS measurements were performed on a VG Instrument type ESCALAB 200R spectrometer equipped with an Al Kα source ($h\nu$ = 1486.6 eV). The shifts of the peak core line due to the charge of the sample were corrected by taking the Al 2p line of the catalyst support, γ-Al$_2$O$_3$ (Al 2p, 74.0 eV) as a reference. For the XPS measurements, the presulfided powder sample was introduced into an argon-filled glove box and pressed on an indium foil fixed on the sample holder under the protection of inert Ar atmosphere. The sample holder was then transferred into the preparation chamber of the XPS equipment and analyzed after evacuation overnight (10^{-9} Pa).

2.3. Catalytic activities measurements

To test the catalytic properties, the hydrodesulfurization reaction of the 4,6-DMDBT model molecule was carried out in a 400 cm^3 batch autoclave magnetically stirred at 593 K under 800 psi (5.516 MPa) total pressure. 200 mg of 4,6-DMDBT model molecule were dissolved in 100 ml of n-dodecane and 200 mg of the sulfided catalyst were used. All reagents were purchased from Sigma–Aldrich.

The reaction was carried out during 8 h and several samples were taken at every 30 min during the first 4 h of the experiment. Then the samples were collected every hour in order to follow the course of the reaction and the transformation of the 4,6-DMDBT.
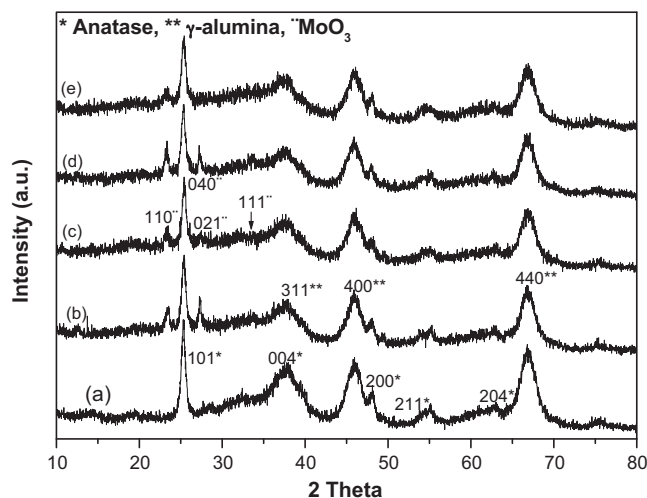

Fig. 1. X-ray diffraction patterns for (a) AT support, (b) Mo/AT, (c) PdMo/AT, (d) NiMo/AT and (e) PdNiMo/AT calcined catalysts.

Samples were analyzed by Gas Chromatography. A 0.25 μm of thickness EC^{TM}-5 (ALTECH) capillary column was used.

In a typical run, the freshly sulfided catalyst was added to the reactor preventing exposure to air by means of a chamber under an argon atmosphere. Then the reactor was heated in a nitrogen atmosphere until the reaction temperature was reached, then it was purged and hydrogen was introduced until the required pressure was attained. At this moment, the reaction was started and the reactant mixture was stirred (1000 rpm).

Previous experiments were performed in order to determine the appropriate conditions and experimental devices in order to avoid reaction control by either intraparticle or interfacial diffusion, in agreement with published work [16].

The products identified throughout the 4,6-DMDBT reaction over all catalysts were 4,6-dimethyltetrahydrodibenzothiophene (4,6-DM-TH-DBT), 3,3'-dimethylbiphenyl (3,3'-DM-BP), 3,3'-dimethy-cyclohexylbenzene (3,3'-DM-CHB) and 3,3'-dimethy-bicyclohexyl (3,3'-DM-BCH).

3. Results and discussion

3.1. X-ray diffraction

X-ray diffraction patterns for the Al$_2$O$_3$–TiO$_2$ support (AT) and Mo/AT, NiMo/AT, PdMo/AT and PdNiMo/AT catalysts calcined at 400 °C are given in Fig. 1. Regarding the AT support, diffraction patterns revealed the presence of γ-Al$_2$O$_3$ (10-0425 PDF) and also the anatase–TiO$_2$ phase (21-1272 PDF). The anisotropic anatase–TiO$_2$ crystallite size was measured of about 40 nm and 25 nm from the (1 0 1) and (2 0 0) reflections respectively. Although the TiO$_2$ concentration is low (about 6 wt.%) the high intensity for the anatase reflections suggests that it was segregated from the alumina and anatase crystallites were randomly dispersed on the alumina matrix. In addition, the γ-Al$_2$O$_3$ alumina crystallite size, measured from the (4 0 0), and (4 4 0) reflections was about 8 nm for both reflections, indicating that the crystallites can be considered isotropic. This support structure was significantly different than other alumina–titania materials reported in the literature [5,6].

XRD patterns for the Mo/AT, NiMo/AT, PdMo/AT and PdNiMo/AT samples calcined at 400 °C exhibited broad reflections belonging to MoO$_3$ with a very low intensity for all the catalysts. This suggests that a fraction of MoO$_3$ was highly dispersed forming small crystallites. However, a low fraction of MoO$_3$ could correspond to larger crystallites. It can also be seen that the crystallite size
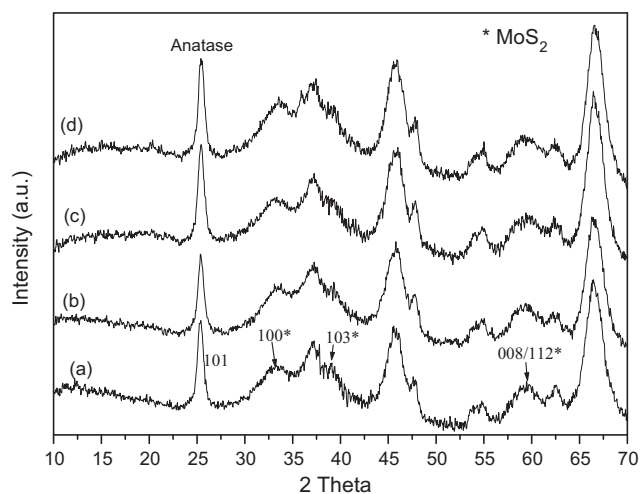
Fig. 2. X-ray diffraction patterns for (a) Mo/AT, (b) PdMo/AT, (c) NiMo/AT and (d) PdNiMo/AT sulfided catalysts.

Fig. 3. Raman spectra for (a) AT support, (b) Mo/AT, (c) PdMo/AT, (d) NiMo/AT and (e) PdNiMo/AT calcined catalysts.

for the anatase–TiO_2 and the (-Al_2O_3 were not affected by the metal impregnation process. Besides, the Ni and Pd oxides were not detected.

XRD results for the sulfided samples are shown in Fig. 2. It was observed that there were broad reflections (0 0 8/1 1 2) corresponding to layered MoS_2 type material for the Mo/AT, NiMo/AT, PdMo/AT and PdNiMo/AT catalysts. The broad MoO_3 reflections disappeared indicating that this species was transformed into MoS_2 species. However, no significant differences were observed for all the series. On the other hand, NiS_x and PdS_x phases were not identified. Moreover, the anatase–TiO_2 phase did not transform into the rutile phase, which is the most thermodynamic stable phase and crystallite size of the anatase–TiO_2 as well as the γ-Al_2O_3 did not grow. This result indicated that the support was stable under the calcination and sulfidation processes.

3.2. Raman spectroscopy

Raman spectra for the AT support and the Mo/AT, NiMo/AT, PdMo/AT and PdNiMo/AT catalysts calcined at 400 °C are shown in Fig. 3. Four peaks at 145 cm^{-1}, 399 cm^{-1}, 520 cm^{-1} and 644 cm^{-1} were observed for all samples and they can be assigned to anatase–TiO_2 particles [17]. The concentrations of MoO_4^{2-}, $Mo_7O_{24}^{6-}$ and $Mo_8O_{26}^{4-}$ species in the impregnation solution depend on the pH among other factors. Since a pH value near 5.6 was used for Mo impregnation, $Mo_7O_{24}^{6-}$ species are expected to be found on the catalysts. A broad band at 956 cm^{-1} was found for all Mo, NiMo, Pd/Mo/NiMo samples (Fig. 3b–e), which can be assigned to the $Mo_7O_{24}^{6-}$ cluster. The Raman band can be attributed to the symmetric and anti symmetric stretching of the Mo=O bonding for molybdenum oxo-species [17]. In addition, PdMo/AT sample presented two bands at 820 and 995 cm^{-1}, indicating that bulk MoO_3 species were also present on the catalyst. This result is in agreement with the X-ray diffraction results. The sample PdNiMo/AT, exhibited two bands at 820 and 956 cm^{-1}, but less intense than for the PdMo/AT solid, suggesting that when Ni is present in the catalysts, MoO_3 dispersion was higher.

3.3. High resolution transmission electron microscopy

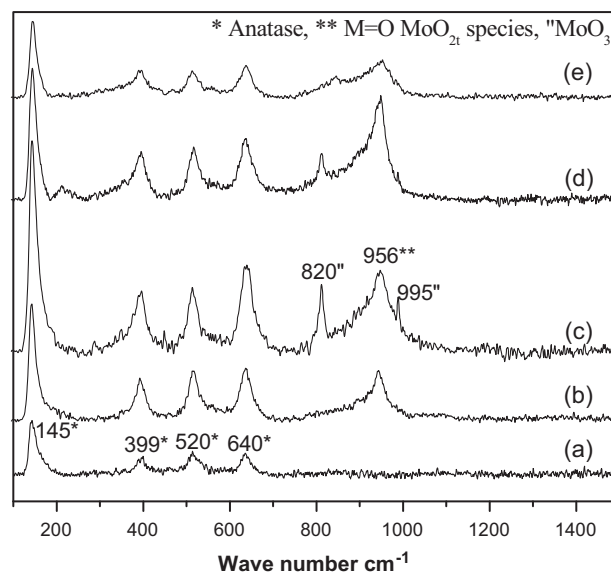HRTEM technique was applied in order to characterize the morphology and dispersion of MoS_2 nanoparticles present on Mo/AT, NiMo/AT, PdMo/AT and NiMoPd/AT sulfided catalysts since both characteristics affect directly the HDS catalytic activity [1]. The representative HRTEM micrographs obtained are shown in Fig. 4. The characteristic slabs for MoS_2 crystallites with 0.61 nm interplanar distances were dispersed over the AT support for all sulfided catalysts. The MoS_2 crystallites were not found growing over the TiO_2 as reported by Shimada [18]. However, MoS_2 crystallites showed different lengths and stacking depending on the composition. They were mainly comprised of 1–4 slabs, with a length between 2 and 8 nm for Mo/AT and PdMo/AT catalysts (Fig. 4a). An important feature is that the MoS_2 slabs were disordered. This result suggests that the incorporation of Pd did not modify MoS_2 morphology and dispersion. By contrast, when Ni was incorporated on the Mo/AT, MoS_2 crystallites with longer slabs and more ordered staking were found for the NiMo/AT and NiMoPd/AT catalyst (Fig. 4b). MoS_2 crystallites observed were comprised of 1–6 slabs, with 2–10 nm long. The complete slabs length distributions for the Mo/AT, NiMo/AT, PdMo/AT and PdNiMo/AT samples are also given in Fig. 5. The promoting effect of Ni seems to modify the AT surface which affects directly the promotion of MoS_2 slabs staking and increasing the length along the low index (1 0 $\bar{1}$ 0) Mo edge or ($\bar{1}$ 0 1 0) S edge. A micrograph where $d_{S–S}$ or $d_{Mo–Mo}$ interatomic distances (0.315 nm) can be measured as well as the interlayer Mo or S distance (0.623 nm) is given in Fig. 4c. A simulated MoS_2 slab with 3 layers and 15 Mo–Mo distances is inserted in the same figure in order to compare directly to the experimental Mo–Mo distances. Nevertheless, it can be clearly observed that there are failures on the MoS_2 interlayer distances along the (1 0 $\bar{1}$ 0) or ($\bar{1}$ 0 1 0) planes and it is possible that these defects can be catalytically active. Regarding Pd or Ni, no individual crystallites were identified on the PdMo/AT, NiMo/AT and NiPdMo/AT respectively. This result suggests that the Pd and Ni are highly dispersed as compared with previous results [15]. Finally, anatase–TiO_2 crystallites were not found, although they were clearly observed by XRD.

EDS chemical analysis was carried out for every sulfided catalysts in order to confirm the presence of Ni and Pd species over the catalysts after the synthesis process (see Fig. 6). It was found that Al, O, Ti elements in the support as well as Mo, Ni, Pd and S were homogeneously dispersed and the chemical composition was also homogenous for all catalysts.
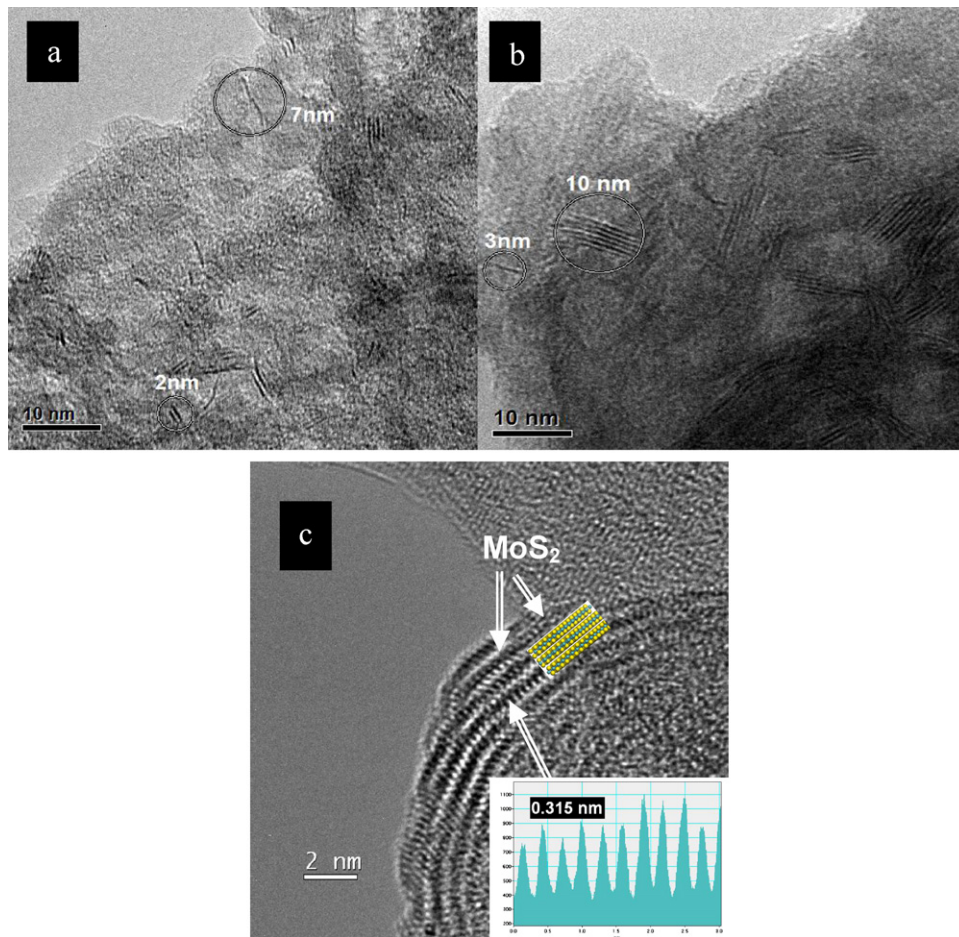
Fig. 4. HRTEM micrographs corresponding for (a) Mo/AT (the morphology is similar to PdMo/AT), (b) NiMo/AT (the morphology is similar to PdNiMo/AT) and (c) higher magnification of MoS_2 morphology and a simulated 3 slabs MoS_2.

3.4. X-ray photoelectron spectroscopy

For all calcined samples, the Mo $3d_{5/2}$ XPS spectra exhibited only a single peak (not shown) with BE ranging from 232.6 to 233.0 eV, which can be assigned to Mo^{6+} species, corresponding probably to MoO_3 (232.6) [19–21]. XPS spectra for Ni $2p_{3/2}$ presented on the catalysts NiMo/AT and PdNiMo/AT showed a single broad and an asymmetric signal, which can be deconvoluted into two peaks

with maxima at 855.5 eV and 857.1 eV (±0.1 eV), characteristic of Ni^{2+} species [22]. The shifting value of 2 eV was significantly different to consider that Ni^{2+} was located in two different chemical environments. However, the Ni $2p_{3/2}$ BE for 855.5 was higher than that reported for Ni $2p_{3/2}$ BE at 854.4 eV which has been assigned to unsupported NiO [20]. It can be suggested that Ni^{2+} was inter-
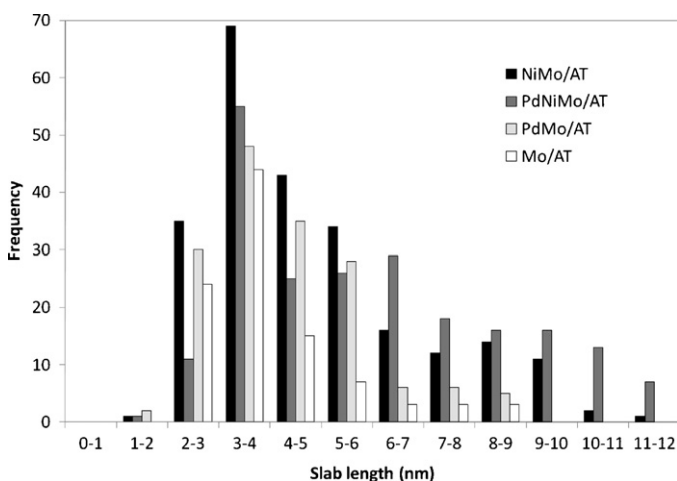

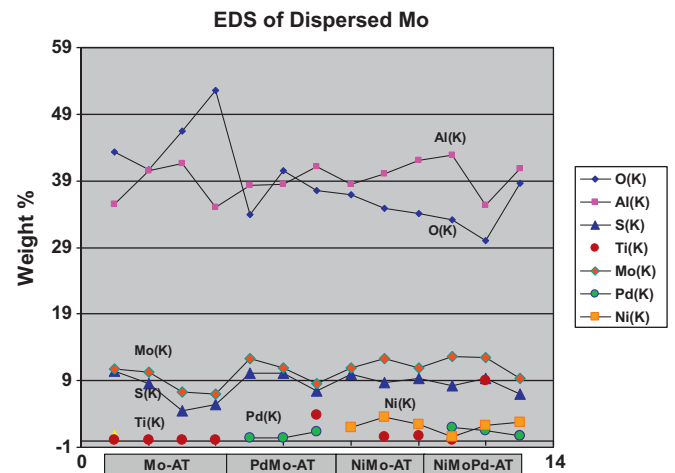**Fig. 5.** MoS_2 slab length distribution for the sulfided catalysts measured by HRTEM.

Fig. 6. EDS chemical analysis for Al, O, Mo, S, Ti, Ni, Pd elements over the sulfided catalysts.
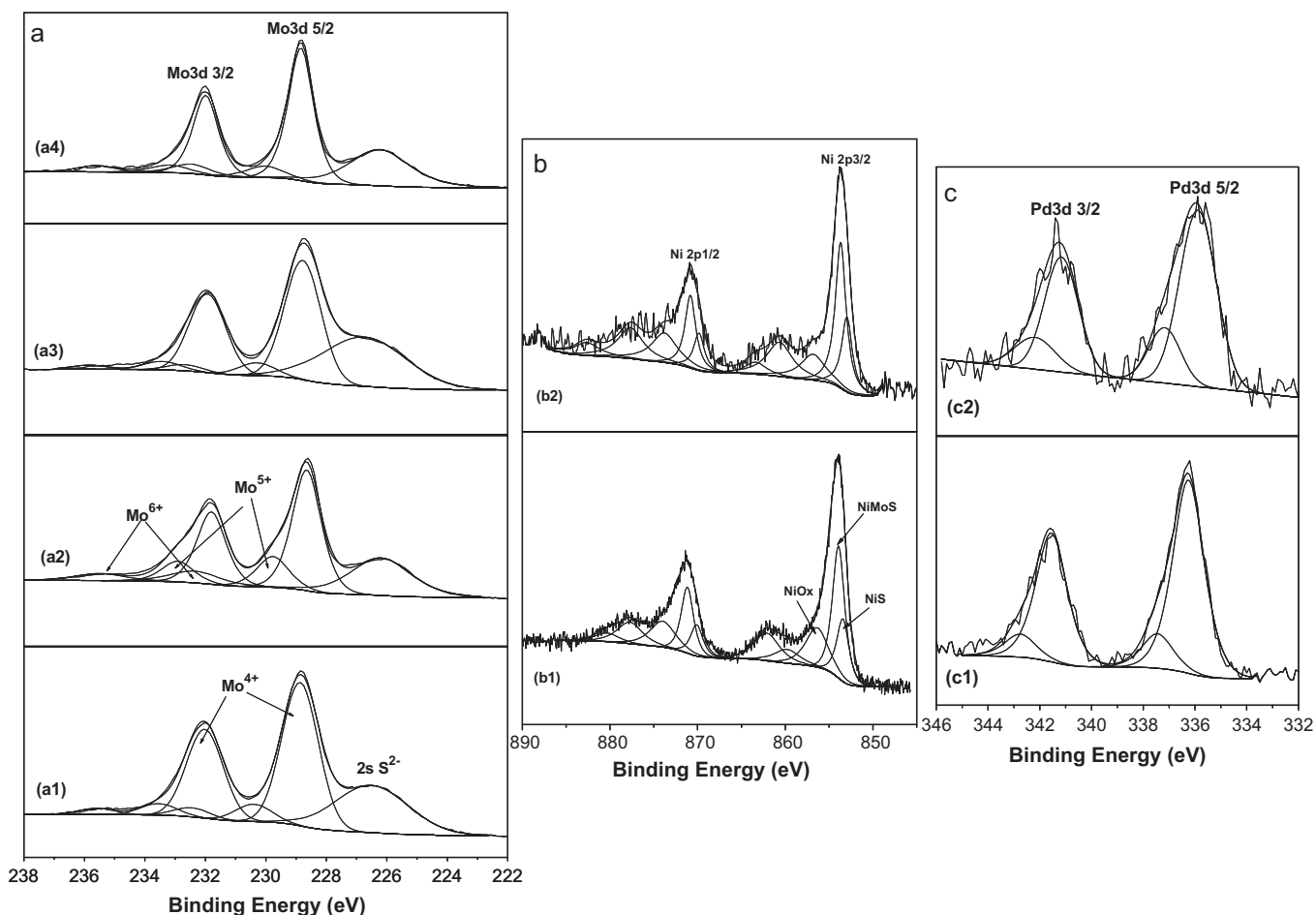
Fig. 7. XPS results for Mo $3d_{5/2}$ and Ni $2p_{3/2}$, on (a1) Mo/AT, (a2) NiMo/AT, (a3) PdMo/AT, (a4) PdNiMo/AT, (b1) NiMo/AT, (b2) PdNiMo/AT, (c1) PdMo/AT and (c2) PdNiMo/AT sulfided catalysts.

acting strongly forming small domains of Al_2NiO_4 (Ni $2p_{3/2}$ BE is 857.00 eV) and Ni^{2+} associated with Mo or as segregated species.

XPS spectra values at the Pd $3d_{5/2}$ level, for the PdMo/AT and PdNiMo/AT catalysts displayed the characteristic doublet of palladium species, at BE 335.4 eV and 337.0 eV. These Pd $3d_{5/2}$ peaks can be assigned to Pd^0 and PdO respectively [19,20]. It suggests that under calcination conditions NH_4 generated by $(NH_4)_6Mo_7O_{24} \cdot 4H_2O$ decomposition at low temperature during the thermal treatment, is enough to reduce about 20% of Pd, since PdO is an easily reducible oxide [8].

For the sulfided catalysts, three peaks in the Mo $3d_{5/2}$ level were found with the BE at about 228.9 eV, 230.3 eV and 232.4 eV (Fig. 7a). The Mo $3d_{5/2}$ at 228.9 eV, has been assigned to that of pure MoS_2 [20,23]. There was a Mo $3d_{5/2}$ peak with BE at 230.3 eV, assigned to Mo^{5+} [24] species. The presence of Mo^{6+} (about 4.0%) on the sulfided catalysts indicated that there was a small fraction of MoO_3. As published extensively, the complete sulfidation of MoO_3 is a difficult task. For instance, it has also been detected unsulfided MoO_3 on different materials, zirconium doped mesoporous silica (Zr/Si) [22], γ-Al_2O_3 [14] and γ-Al_2O_3 dopped with Ga [25].

The Ni 2p core level signal for Ni promoted sulfided catalysts NiMo/AT and PdNiMo/AT were deconvoluted into three components at 853.9 (main peak), 853.4 and 854.8 eV (see Fig. 7b). The main peak located at 853.6 can be assigned to Ni in the NiMoS phase, while the peak at 853.4 eV can be attributed to NiS and the peak at 854.8 can be attributed to NiOx species. The satellite shake-up lines at higher binding energies remained in the sulfided catalysts due to the remaining Ni^{2+} cations immersed in an oxidative environment, probably forming Al_2NiO_4 or $NiTiO_3$ small domains [22].

XPS spectra for Pd $3d_{5/2}$ level for the PdMo/AT and PdNiMo/AT sulfided catalysts, exhibited a sharper peak than that found on the corresponding calcined catalysts (see Fig. 7c). The deconvolution showed two peaks with maxima at 336.3 eV (67%) and 337.2 eV (13%) binding energies. The highest peak, at 336.3 eV BE, is shifted towards lower energy in comparison with that for PdO (337.4 eV) and higher than that for the Pd^0 (335.4 eV), thus it can be proposed that a PdS_x species was formed. It can also be suggested that a fraction of the Pd atoms would be interacting strongly with alumina or titania support forming PdOx structures.

3.5. Catalytic activities and products yields

The initial rates for HDS are shown in Fig. 8 for all catalysts. A comparison between reaction rates for monometallic Mo/A and Mo/AT catalysts showed that the value for the latter was 2 times higher than that for the former. When adding Ni to both catalysts, a significant increase in the reaction rate was observed. A promoting effect can be calculated by dividing the reaction rate for the NiMo samples by the Mo activity for each catalyst deposited on the same carrier. The promotion effect was found to be equal to 12 for the NiMo/A and equal to 7 for the NiMo/AT with respect to the Mo/A and Mo/AT samples respectively. This difference in promoting effect was already been reported for alumina–titania supported samples [26]. Interestingly, the NiMo/AT catalyst was more active than the NiMo/A sample. The activity for the Pd/AT sample was added as reference and it displayed a low activity as compared with the Mo/AT sample. However, the Pd content was very low (3 wt.%). By contrast, the incorporation of Pd (0.3 wt.%) over the
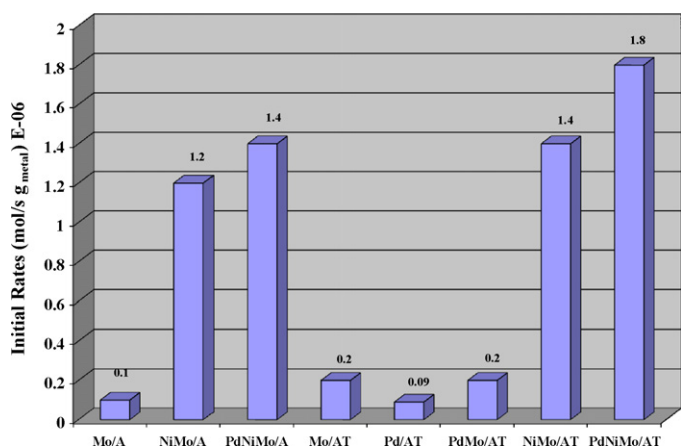
Fig. 8. Initial rates for the hydrodesulfurization of 4,6-dimethyldibenzothiophene at 593 K and 800 psi over Mo/A, NiMo/A, Mo/AT, PdMo/AT, NiMo/AT and PdNiMo/AT sulfided catalysts.

Mo/AT sample did not show any significant increase in reaction rate. This result is in agreement with previous findings about the Pd effect on the HDS activity for Mo catalysts supported on alumina [7,14].

Pd incorporation over the NiMo/A and NiMo/AT sample increased the reaction rate by ca. 16 and 30% respectively and the PdNiMo/AT catalyst exhibited the highest activity. These results point out to a promoting effect by Pd. Pessayre et al. [13] published a decrease in the DBT conversion when adding Pt to a NiW oxide sample supported on alumina but an increase in this value when the addition of Pt was carried out to a sulfided solid. Furthermore, Navarro et al. [14] did not report any difference in HDS conversion when adding Pd to NiMo sulfide catalyst supported on alumina. Thus, the alumina–titania carrier should be playing an important role in the promotion of Pd on the NiMo system.

The characteristic molecule coming from the hydrogenolysis or direct desulfurization route (DDS) was the 3,3′-dimethylbiphenyl (3,3′-DM-BP) and the desulfurization molecules produced by the hydrogenation route (HYD) were 3,3′-DM-CHB and the totally hydrogenated 3,3′-DM-BCH. Fig. 9 depicts the products yields as a function of the 4,6-DMDBT conversion for the Mo/A and Mo/AT catalysts. It can be seen that the main compound was 4,6-DM-TH-DBT hydrogenated intermediate and its yield increased with conversion. The selectivity to the desulfurized products 3,3′-DM-BP (DDS), 3,3′-DM-CHB (HYD) and 3,3′-DM-BCH (HYD) throughout the reaction was quite similar for both catalysts (see Fig. 9a and b). However, the selectivity towards the 3,3′-DM-CHB by sulfur elim-
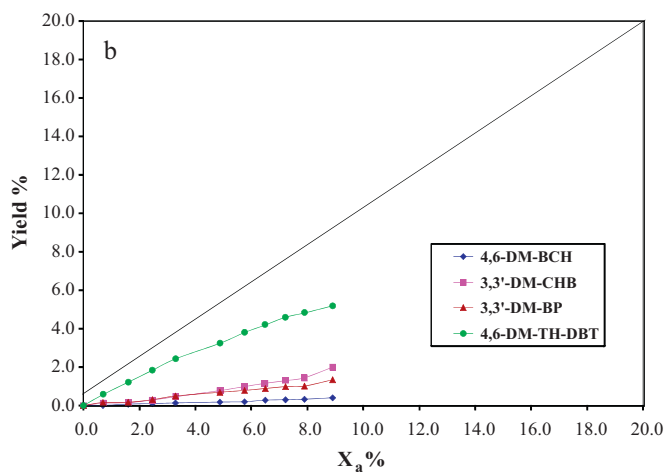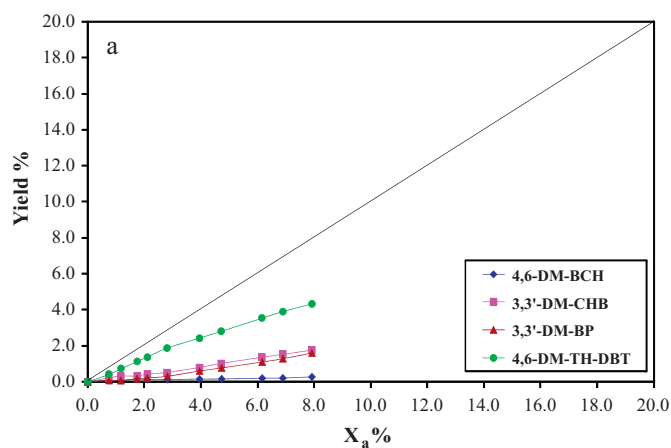

Fig. 9. Products distribution (yield%) for the hydrodesulfurization of 4,6-dimethyldibenzothiophene over (a) Mo/A and (b) Mo/AT sulfided catalysts.
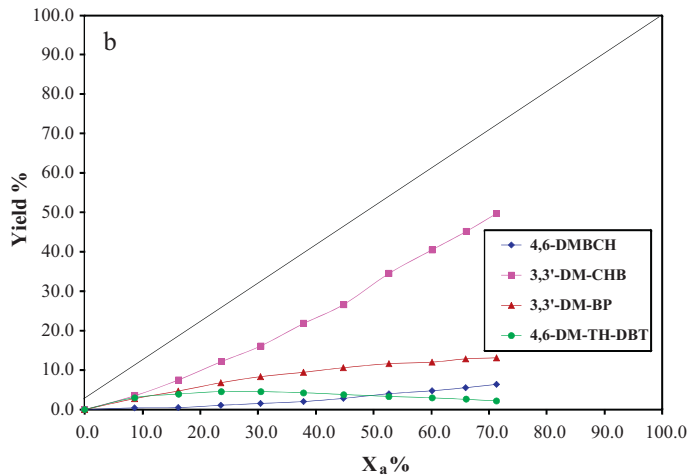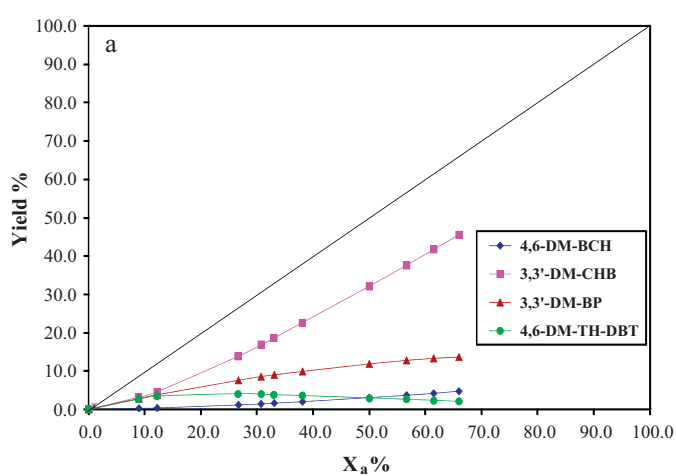

Fig. 10. Products distribution (yield%) for the hydrodesulfurization of 4,6-dimethyldibenzothiophene over (a) NiMo/A and (b) NiMo/AT sulfided catalysts.
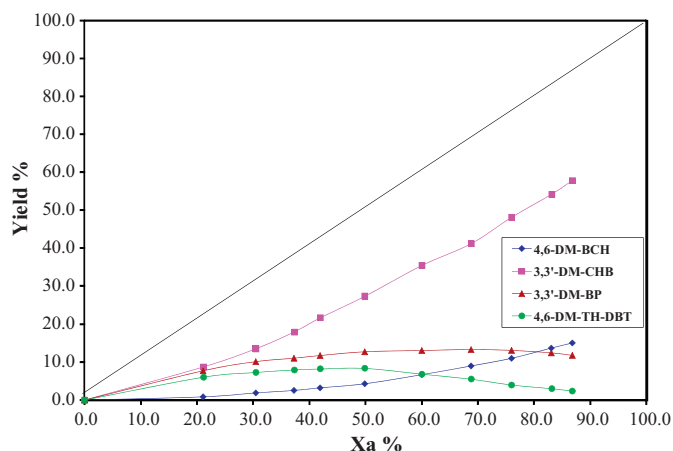
Fig. 11. Products distribution (yield%) for 4,6-dimethyldibenzothiophene hydrodesulfurization reaction over the PdNiMo/AT sulfided catalyst.

ination (HYD) was slightly higher than 3,3′-DM-BP (DDS) for both catalysts. The complete saturated and desulfurized 3,3′-DM-BCH (HYD) compound was practically constant. The addition of Pd to the Mo/AT catalysts did not show any significant differences in product yields as compared with the Mo/AT sample (figure not shown).

For the NiMo/A and NiMo/AT catalysts the product distribution patterns are shown in Fig. 10. One can notice significant differences with those for the unpromoted systems. For both catalyst the main compound produced was the desulfurized 3,3′-DM-CHB (HYD). According to the literature [2] this compound comes basically from the C–S cleavage of the partially hydrogenated 4,6-DM-TH-DBT compound, which suggests that the main effect of Ni over the Mo catalysts was to accelerate the hydrogenation of the 4,6-DM-TH-DBT intermediate. Furthermore, the DDS route was also favored for the NiMo samples as higher production for 3,3′-DM-BP was observed. However product yields for the HYD pathway were higher than the DDS pathway. Fig. 11 shows that the PdNiMo/AT catalyst presents a very similar distribution product pattern throughout the reaction as the NiMo catalysts. Nevertheless a slightly higher yield for 3,3′-DM-BCH (HYD) compound was noticed at conversions up to 50% while the 4,6-TH-DMDBT decreased.

From catalytic properties results it appeared that Pd did not enhance either the activity or selectivity for Mo supported on alumina–titania and it can be explained in terms of a lack of promotion of Pd over MoS_2 sites. From Raman Spectroscopy on the calcined samples, MoOx species were not modified and XRD showed significantly larger particles than for NiMo/AT. Moreover, stacking and length of MoS_2 crystallites determined from HRTEM results, did not vary after Pd addition and Pd particles were not detected by this technique. These results suggest that Pd could be well dispersed on the alumina–titania surface without any significant electronic interaction with the MoS_2 phase. By contrast, XRD and Raman results pointed out to a different interaction between Pd and the NiMo/AT system. Firstly, MoOx particles exhibited smaller particles which were almost completely sulfided. Secondly, HRTEM images showed an increase in order and stacking after Pd addition as compared with Mo/AT. Finally, the total hydrodesulfurization capacity for the PdNiMo/AT was higher than that for Mo/AT and NiMo/AT, suggesting a close interaction of Pd with NiMo. Furthermore, since Pd promoted the HDS activity for a NiMo system supported on AT as compared with an equivalent catalyst supported on A, the support played an important role. It should be

mentioned that most of the previous papers reported no gain of catalytic activity when Pd was incorporated in the oxide state to NiMo or NiW catalysts supported on alumina. The anatase phase is recognized to prevent Ni migration into the support and it has also been reported that it exerts a positive electronic interaction with Pd [27].

4. Conclusions

The addition of Pd and Ni over the Mo/AT had a positive effect and produced highly active sulfided catalyst for hydrodesulfurization of the highly refractory 4,6-DMDBT molecule by enhancing both the hydrogenation and hydrodesulfurization pathways. There was found a synergetic effect of Pd and Ni on the Mo/AT catalyst, but it is higher when Pd is incorporated on NiMo/AT catalyst than when Pd is incorporated on Mo/AT catalyst. From our results, since Pd promoted the HDS activity for a NiMo system, the alumina–titania support played an outstanding role over the incorporation to Pd to the active phases.

References

[1] H. Topsoe, B.S. Clausen, F.E. Massoth, in: J.R. Anderson, M. Boudart (Eds.), Catalysis Science and Technology, vol. 11, 1996.
[2] F. Bataille, J.L. Lemberton, P. Michaud, G. Pérot, M. Vrinat, M. Lemaire, E. Schulz, M. Breysse, S. Kasztelan, J. Catal. 191 (2000) 409.
[3] A. Stanislaus, B.H. Cooper, Catal. Rev. -Sci. Eng. 36 (1994) 75.
[4] T. Mochizuki, H. Itou, M. Toba, Y. Miki, Y. Yoshimura, Energy Fuels 22 (2008) 1456.
[5] I.R. Galindo, J.A. de los Reyes, Fuel Process. Technol. 88 (2007) 859.
[6] S. Nuñez, A. Montesinos-Castellanos, T.A. Zepeda, J.A. los Reyes, Mater. Res. Innovations 12 (2008) 55.
[7] L.I. Meriño, A. Centeno, S.A. Giraldo, Appl. Catal. A: Gen. 197 (2000) 61.
[8] V.L. Barrio, P.L. Arias, J.F. Cambra, M.B. Guemez, B. Pawelec, J.L.G. Fierro, Fuel 82 (2003) 501.
[9] Z. Vít, D. Gulková, L. Kaluza, M. Zdrazil, Appl. Catal. 272 (2004) 99.
[10] Z. Vít, D. Gulková, L. Kaluza, M. Zdrazil, J. Catal. 232 (2005) 447.
[11] D. Gulková, Y. Yoshimura, Z. Vít, Appl. Catal. B: Environ. 87 (2009) 171.
[12] Y. Yoshimura, M. Toba, T. Matsui, M. Harada, Y. Ichihashi, K.K. Bando, H. Yasuda, H. Ishihara, Y. Morita, T. Kameoka, Appl. Catal. A: Gen. 322 (2007) 152.
[13] S. Pessayre, C. Geantet, R. Bacaud, M. Vrinat, T.S. N'Guyen, Y. Soldo, J.L. Hazemann, M. Breysse, Ind. Eng. Chem. Res. 46 (2007) 3877.
[14] R.M. Navarro, P. Castaño, M.C. Álvarez-Galván, B. Pawelec, Catal. Today 143 (2009) 108.
[15] T. Klimova, P. Mendoza Vara, I. Puente Lee, Catal. Today 150 (2010) 171.
[16] J. Escobar, M.C. Barrera, J.A. de los Reyes, J.A. Toledo, V. Santes, J.A. Colín, J. Mol. Catal. A: Chem. 287 (2008) 33.
[17] I.E. Wachs, Catal. Today 27 (1996) 437.
[18] H. Shimada, Catal. Today 86 (2003) 17.
[19] D. Briggs, M.P. Seah (Eds.), Practical Surface Analysis. Auger and X-Ray Photoelectron Spectroscopy, Wiley, New York/Salle and Sauerlander, 1990.
[20] http://srdata.nist.gov/xps/, NIST NIST X-ray Photoelectron Spectroscopy (XPS) Database version 3.5 on line.
[21] C.V. Cáceres, J.L.G. Fierro, J. Lazaro, A.L. Agudo, J. Soria, J. Catal. 122 (1990) 113.
[22] E. Rodríguez-Castellón, A. Jiménez-López, D. Eliche-Quesada, Fuel 87 (2008) 1195.
[23] I. Alstrup, I. Chorkendorff, R. Candia, Bs. Clausen, H. Topsøe, J. Catal. 77 (1982) 397.
[24] E. Altamirano, J.A. de los Reyes, F. Murrieta, M. Vrinat, J. Catal. 235 (2005) 403.
[25] E. Altamirano, J.A. de los Reyes, F. Murrieta, M. Vrinat, Catal. Today 133–135 (2008) 292.
[26] E. Olguín, M. Vrinat, L. Cedeño, J. Ramírez, M. Borque, A. López-Agudo, Appl. Catal. A: Gen. 165 (1997) 1.
[27] S. Nuñez, J. Escobar, A. Vázquez, J.A. de los Reyes, M. Hernández-Barrera, Mater. Chem. and Phys. 126 (2011) 237.